LANGMUIR

pubs.acs.org/Langmuir Article

Meso- and Macroporous Polymer Gels for Efficient Adsorption of Block Copolymer Surfactants

Pratik S. Gotad, Navin Kafle, Toshikazu Miyoshi, and Sadhan C. Jana*



Cite This: Langmuir 2022, 38, 13558-13568



ACCESS

III Metrics & More

Article Recommendations

s Supporting Information

ABSTRACT: An understanding of surfactant adsorption at solid—liquid interfaces is important for solving many technological problems. This work evaluates surfactant adsorption abilities of high surface area (200–600 m²/g), high porosity (>90%), hierarchically structured open pore polymer gels. Specifically, the interactions of a nonionic block copolymer surfactant, poly(ethylene oxide)—poly(propylene oxide)—poly(ethylene oxide) (PEO-PPO-PEO), with three polymer gels, namely, syndiotactic polystyrene (sPS), polyimide (PI), and polyurea (PUA) offering different surface energy values, are evaluated at surfactant concentrations below and well above the critical





Monolayer adsorption at

Micelle confinement at Chulk > C_{CMC}

micelle concentration (CMC). Two distinct surfactant adsorption behaviors are identified from the surface tension and nuclear magnetic resonance data. At concentrations below CMC, the surfactant molecules adsorb as a monolayer on polymer strands, inferred from the Langmuir-type adsorption isotherm, with the adsorbed amount increasing with the specific surface area of the polymer gel. The study reports for the first time that the gels show a strong surfactant adsorption above CMC, with the effective surfactant concentration in the gel reaching several folds of the CMC values. The effective surfactant concentration in the gel is analyzed using surfactant micelle size, polymer surface energy, and pore size of the gel. The findings of this study may have strong implications in liquid—liquid separation problems and in the removal of small dye molecules, heavy metal ions, and living organisms from aqueous streams.

1. INTRODUCTION

An understanding of surfactant adsorption at solid-liquid interfaces is essential to solving many technological problems. Oil—water emulsion separation, 1,2 modification of surfaces or wettability of solid surfaces, 4 surfactant-aided membrane processes such as micellar liquid chromatography, 5 and micellar-enhanced ultrafiltration⁶ are a few examples that benefit from surfactant adsorption studies. Published literature often focuses on adsorption of surfactants on conventional solid substrates such as flat surfaces^{7,8} or spherical particles.^{9,10} In this context, very limited literature exists on surfactant adsorption on solid substrates, with inherent porous structures presenting confined geometries. Prior work established that molecular transport and adsorption-desorption processes at the nanoscale are different from those observed for bulk, micrometer-sized solid substrates. 11 Mesoporous silica gels with pores in the 2 to 50 nm range exhibit an array of interactions with various ionic and nonionic surfactant systems. $^{12-15}$ For example, at concentrations below the critical micelle concentration (CMC), the surfactant molecules show aggregative adsorption at the solid-water interfaces. 12 This aggregation follows a two-step process. In the first step, the surfactant molecules anchor onto the polymer surfaces by hydrophobic-hydrophobic or hydrogen-bonding interactions. In the second step, surfactant molecules organize into aggregates via lateral interactions 16 in the form of hemimicellar, micellar, or bilayer structures. However, to the best of our knowledge, a similar study does not exist on surfactant

adsorption in polymer gel systems. This study advances understanding of the underlying physics of surfactant adsorption in the confined pores of polymeric materials with a pore diameter in the 10 to 200 nm range and polymer substrates offering different levels of surface energy and specific surface area.

We note that polymer gels differ from silica gel systems in surface chemistry, polarity, pore sizes, and the architecture of solid surfaces; for example, typical polymer gels have strands of a few tens of nanometers in diameter compared to spherical silica particles of 1 to 5 nm in diameter with plenty of surface silanol groups. A majority of polymer gels reported to date are hierarchically porous, with interconnected networks of mesopores (2 to 50 nm in diameter) and macropores (diameter > 50 nm). $^{17-20}$ In conjunction, the polymer gels offer a high specific surface area $(200-800~{\rm m}^2/{\rm g})^{21-23}$ that can be leveraged for high amounts of surfactant adsorption. It is imperative, therefore, that studies on surfactant adsorption behavior in porous polymer gel systems may yield interesting observations that can advance the understanding of several

Recived: August 14, 2022 Revised: October 12, 2022 Published: October 24, 2022





liquid—liquid separation problems, for example, using porous polymer gels as adsorbents.

Several porous gel-forming polymer systems have been reported in the literature, such as syndiotactic polystyrene (sPS), 21,24 polyimide (PI), 22,25 polyurea (PUA), 18 polyurethane, 26 and cellulose, 19 to name a few. The corresponding aerogels obtained by supercritical drying of the gels provide a high surface area (250–800 m²/g) and high porosity (>90%). Extensive work shows that pore size 22,23,27 and wettability 28 can be tuned, and the gels can be fabricated into various shapes and sizes $^{29-31}$ to suit the desired applications of aerogels, such as thermal insulation, 32 air filtration, 20,33 and dye removal from wastewater streams. 29

The three polymer gels used in this work are sPS, PI, and PUA. All three gels offer high porosity with hierarchical porous structures composed of meso- and macropores. However, PI offers the highest mesopore fraction, while sPS gels contain primarily macropores. The three polymer systems also differ in surface energy values, thus, presenting different levels of interactions with surfactants. sPS gels are formed by a thermoreversible gelation mechanism of sPS in a good solvent.34,35 The inherent tacticity of sPS allows a rapid gelation by the spinodal decomposition route when the sPS solution is quenched. Daniel et al. reported the sPS aerogel first in 2005.³⁴ Both PI and PUA gels are formed by chemical crosslinking of the respective monomer systems. A two-step reaction process is used for polyimide gels.³⁶ In the first step, selected diamine and dianhydride molecules react to form a linear polyamic acid. In the second step, a trifunctional crosslinker is used, along with acetic anhydride and pyridine, to convert polyamic acid into a polyimide gel with three-dimensional polymer networks. ^{17,37} PUA aerogels were first reported in a United States patent by Biesmans et al.³⁸ The PUA-based gels are synthesized by reacting an isocyanate with water in the presence of a catalyst. 23,39,40

In this work, the interactions of poly(ethylene oxide)—poly(propylene oxide)—poly(ethylene oxide) (PEO-PPO-PEO) block copolymer surfactants with three polymer gels in the form of sPS, PI, and PUA were studied. It was hypothesized that the surface energy of the polymer constituting the gel would play a significant role in deciding surfactant adsorption at the polymer—water interface. As will be seen later, sPS, PI, and PUA gels offered similar porosity values, pore morphology, and interconnected porous structures, but different surface energy values.

The PEO-PPO-PEO block copolymer surfactant was chosen for its significance in emulsion science, drug delivery, and surface modification. Significant prior work exists in the literature on adsorption of ionic surfactants, but studies on nonionic surfactants are limited. The surfactant adsorption by the gels at below CMC and well above CMC was studied. As will be seen, the PEO-PPO-PEO block copolymer surfactant produced different sized micelles that were useful for investigation of surfactant adsorption behavior at concentration regimes above CMC. The influence of surfactant micelle sizes and polymer gel pore sizes on surfactant-adsorbed amounts by gels were investigated. The results of this study present an important first step toward the understanding of demulsification of oil—water emulsion systems using high surface area polymer gels.

2. EXPERIMENTAL SECTION

2.1. Materials. sPS ($M_{\rm w} \approx 300000$ g/mol, 98%) was obtained from Scientific Polymer Producers Inc. (Ontario, NY, U.S.A.). 2,2'-Dimethylbenzidine (DMBZ) was purchased from Shanghai Worldyang Chemical Co. Ltd. (Shanghai, China). Pyromellitic dianhydride (PMDA, \geq 96.5%), tris(2-aminoethyl) amine (TREN, \geq 95.5%) crosslinker, acetic anhydride (≥99%), and toluene (≥99.9%) were purchased from Sigma-Aldrich (Milwaukee, WI, U.S.A.). Pyridine $(\geq 99\%)$ and acetone $(\geq 99.5\%)$ were purchased from Fisher Scientific (Ontario, NY, U.S.A.). N_iN -Dimethylformamide (DMF, $\geq 99.5\%$) was purchased from VWR International (Radnor, PA, U.S.A.). Ethanol was purchased from Decon Laboratories Inc. (King of Prussia, PA, U.S.A.). Desmodur N3300A (tri-isocyanate) and triethyl amine (TEA) were procured from Covestro (Pittsburgh, PA) and Sigma-Aldrich (Milwaukee, WI, U.S.A.), respectively. Three different PEO-PPO-PEO surfactants were used in this work, namely, Pluronic L35, Pluronic P123, and Pluronic F-127, with molecular weights of 1900, 5800, and 12600 g/mol, respectively, and a PEO content of 50, 30, and 70 wt %, respectively. All these surfactants were procured from Sigma-Aldrich (Milwaukee, WI, U.S.A.). Deuterium oxide (D₂O, deuteration degree min ≥ 99.95%) was purchased from Sigma-Aldrich (Milwaukee, WI, U.S.A.). All the chemicals were used without further purification.

2.2. Fabrication of sPS Gels and Aerogels. sPS gels were obtained by thermoreversible gelation of solutions of sPS in toluene. The solutions were prepared by dissolving sPS in toluene in sealed vials at 100 °C at a solid concentration of 0.06 g/mL and allowed to cool under ambient conditions for 1 min. The solutions were then poured into a covered cylindrical glass mold with a diameter of 15 mm for gelation. The gels were allowed to stand in the mold for 5 h to ensure complete gelation, demolded, and solvent-exchanged first with ethanol and finally with deionized (DI) water to obtain water-filled sPS gels for the next steps.

The ethanol-filled sPS gels were solvent-exchanged with liquid carbon dioxide and dried under supercritical conditions of carbon dioxide at 50 °C and 11 MPa pressure to recover solid sPS aerogels. The aerogels were used for the evaluation of surface energy and examination of pore size.

2.3. Fabrication of PI Gels and Aerogels. PMDA and DMBZ were dissolved separately in DMF, and the solutions were mixed together at room temperature under magnetic stirring for 2 min at 1200 r.p.m. to form a linear polyamic acid solution in DMF. Subsequently, TREN, acetic anhydride, and pyridine were added to polyamic acid solution and magnetically stirred for 3 min. The final solution was poured into a cylindrical mold with a diameter of 16 mm, and gelation occurred within 10 min. The gels were aged in the mold for 24 h and solvent-exchanged with mixtures of DMF and acetone in ratios of 75:25, 50:50, 25:75 v/v, followed by three additional solvent exchange steps with 100% acetone. The acetone in the gels was then exchanged with liquid carbon dioxide and dried under the supercritical conditions of carbon dioxide at 50 °C and 11 MPa pressure to obtain aerogels. The water-filled PI gels were obtained by the solvent-exchange of gels filled with acetone using acetone-DI water mixtures of increasing water concentration and finally with 100% DI water. PI gels of 7.5 wt % polymer concentration were obtained from 0.686 g of PMDA, 0.636 g of DMBZ, 92 µL of TREN, 1.847 mL of acetic anhydride, and 1.909 mL of pyridine in 15 mL of DMF.

2.4. Fabrication of PUA Gels and Aerogels. The tri-isocyanate was first dissolved in DMF at room temperature with magnetic stirring, followed by mixing with DI water for 3 min and additional mixing for 2 min after TEA was added. The mixture was transferred to a cylindrical mold with a diameter of 15 mm and allowed to stand and gel at room temperature for 50–60 min, followed by 24 h of aging in the mold. The PUA gels were synthesized using tri-isocyanate, water, and TEA in a molar ratio of 1:3:1 with a 0.15 M concentration of tri-isocyanate. The PUA gels filled with acetone and suitable for supercritical drying were obtained by solvent exchanging in steps with mixed solvents DMF—acetone in ratios of 75:25, 50:50, 25:75 v/v,

followed by three solvent exchanges in 100% acetone. The acetone-filled gels were solvent exchanged in liquid $\rm CO_2$ and subsequently dried under supercritical conditions of $\rm CO_2$ at 50 °C and 11 MPa pressure to obtain aerogels. Deionized water-filled gels were obtained by exchanging acetone in acetone-filled gels with acetone—water mixtures with increasing concentrations of DI water and finally with only DI water.

2.5. Characterization. 2.5.1. Surfactant Adsorption. The amount of surfactant adsorbed by water-filled gels from a solution of surfactant of concentration of 0–15 wt % in DI water was determined after allowing the polymer gel of known mass to be dipped in the solution to equilibrate over a period of 24 h at room temperature. The value of the surface tension (σ) of water was determined before and after dipping the gel, and the concentration of the surfactant in water after adsorption by the gel was determined from the calibration curve of σ versus surfactant concentration. It is noted that at above the CMC, σ assumes a constant value $(\sigma_{\rm CMC})$. Such solutions were diluted to below CMC by adding known aliquots of DI water until the value of σ was found greater than $\sigma_{\rm CMC}$. All adsorption experiments were repeated thrice for each data point. In this work, σ was obtained from the pendant drop method using the drop shape analyzer (DSA25S, Krüss GmbH, Germany).

2.5.2. ¹H NMR. Solution ¹H NMR data were obtained for the precise characterization of the surfactant concentration within the polymer gel, especially at surfactant concentrations above CMC. The polymer gels were dipped in an aqueous surfactant solution of known initial concentration for a period of 24 h. Subsequently, 0.6 g of polymer gel was inserted into the NMR tube and filled with 0.5 mL of deuterium oxide (D_2O) used as the solvent. The H_2O/D_2O ratio was approximately 1:1. Solution-state ¹H NMR spectra were recorded on an Agilent NMR 500 MHz (Santa Clara, CA) at 298 K. A 90° pulse of 14.12 μs was used to excite ¹H NMR signals. Accumulation number and recycle delay were set to 64 and to 5 s, respectively. ¹H spinlattice relaxation time in the laboratory frame (T_1) was measured by inversion recovery method for 0.1 and 15 wt % Pluronic L35 aqueous surfactant solutions. T_1 relaxation time for the water peak was found to be 0.9 s and those for the surfactant peaks at 3.63, 3.5, and 1.1 ppm were found to be 0.8, 0.55, and 0.70 s, respectively, and hence, the recycle delay was set to 5 s to ensure complete relaxation of all the proton signals. Under such condition, the NMR spectroscopy data produced quantitative measure of surfactant concentration within the polymer gel.

2.5.3. Bulk Density, Skeletal Density, and Porosity Measurements. The bulk density $(\rho_{\rm b})$ of aerogel specimens was measured from mass and volume while the skeletal density $(\rho_{\rm s})$ was obtained from Helium pycnometer (AccuPyc II 1340, Micromeritics Instrument Corp., Norcross, GA). The porosity $(\rho_{\rm T})$ of the aerogel specimens was calculated using eq 1.

$$\rho_{\mathrm{T}} = (1 - \rho_{\mathrm{b}}/\rho_{\mathrm{s}}) \times 100 \tag{1}$$

2.5.4. Brunauer-Emmett-Teller (BET) Adsorption-Desorption. The specific surface area and mesopore volume $(V_{
m meso})$ of aerogel specimens were obtained from BET analysis of N2 adsorptiondesorption isotherms obtained at 77 K using a Micromeritics Tristar II 3020 analyzer (Micromeritics Instrument Corp., Norcross, GA). The BET isotherm was obtained at 77 K to improve the detection accuracy of the instrument for nitrogen adsorption. It is noted that the specific surface area reported in the manuscript corresponded to that of the aerogels, although surfactant adsorption experiments were conducted using corresponding gels with slightly higher pore volumes. The volume shrinkage of the gel during supercritical drying in all cases was small, around 10% and the specific surface area reported for aerogels come close to that in the gel state. The macropore (diameter > 50 nm) volume ($V_{\rm macro}$) was obtained from the difference of total pore volume ($V_{\rm total}$ eq 2) and sum of $V_{\rm meso}$ and micropore volume $(V_{
m micro})$. Since the micropore volume fraction for the gels utilized in this work was extremely low (≤ 0.01), we considered it negligible for our purpose.²² The nonlocal density functional theory (NLDFT) model was used to obtain the mesopore volume fraction from N2 isotherms at 77 K. The total pore volume and fraction of meso $(\phi_{\rm meso})$ and macropores $(\phi_{\rm macro})$ were calculated using eqs 2–4. The pore size distribution was obtained using the Barrett–Joyner–Halenda (BJH) analysis of nitrogen isotherms.

$$V_{\text{total}} = \frac{1}{\rho_{\text{b}}} - \frac{1}{\rho_{\text{s}}} \tag{2}$$

$$\phi_{\rm meso} = \frac{V_{\rm meso}}{V_{\rm total}} \tag{3}$$

$$\phi_{\text{macro}} = \frac{V_{\text{macro}}}{V_{\text{total}}} = 1 - \phi_{\text{meso}} \tag{4}$$

2.5.5. Contact Angle and Surface Energy of Polymer Specimens. The water contact angle on compressed aerogel discs was measured using sessile drop method and analyzed using Kruss drop shape analyzer. For this purpose, aerogel specimens were compressed as discs between two clean, flat metal platens at 13.8 MPa pressure to remove the pores so that only the chemistry of the polymer affects the contact angle values. In each measurement, a water droplet of 10 μ L volume was placed on the surface of the compressed disc. The contact angle between water and the polymer surface was read from the optical image using ImageJ software.

The surface energy of polymer specimens and its polar and dispersive components were calculated using Wu's theory⁴² as per eq 5. For this purpose, the contact angle values of water and diiodomethane were measured on compressed polymer disks.

$$\gamma_{LS} = \gamma_{L} + \gamma_{S} - \frac{4\gamma_{L}^{d}\gamma_{S}^{d}}{\gamma_{L}^{d} + \gamma_{S}^{d}} - \frac{4\gamma_{L}^{p}\gamma_{S}^{p}}{\gamma_{L}^{p} + \gamma_{S}^{p}}$$
(5)

In eq 5, γ_{LS} is the interfacial tension between liquid and solid, γ_L is the surface tension of the liquid, γ_S is the surface energy of the solid, and γ^d_S and γ^p_S are the dispersion (nonpolar) and polar components of liquid surface tension, respectively. The standard values of $\gamma_L^d=21.8$ dyn/cm and $\gamma_L^p=50.7$ dyn/cm for water and $\gamma_L^d=44.1$ dyn/cm and $\gamma_L^p=6.7$ dyn/cm for diiodomethane were used in the calculations. The surface energy of polymer is obtained from the sum of dispersive (γ^d_S) and polar (γ^p_S) components as in eq 6.

polymer surface energy(
$$\gamma_{\rm S}$$
) = $\gamma_{\rm s}^{\rm d} + \gamma_{\rm s}^{\rm p}$ (6)

The polymer–liquid interfacial energy (γ_{LS}) was calculated using Young–Laplace equation, as in eq 7, where γ_L is surface tension of the liquid and θ is the contact angle on polymer surface.

$$\gamma_{\rm S} = \gamma_{\rm LS} + \gamma_{\rm L} \cos \theta \tag{7}$$

2.5.6. Morphology. The morphology of aerogel specimens was examined using scanning electron microscope (SEM JSMS310, JEOL,MA).

2.5.7. Dynamic Light Scattering (DLS). The size of micelles of surfactants in DI water was determined using DLS at 25 °C. For this purpose, 5 wt % surfactant solution was prepared in deionized water and analyzed using Zetasizer Nano ZS90 (ZEN3690, Malvern Instruments Limited, Worcestershire, U.K.).

2.5.8. Surfactant Desorption. Syndiotactic polystyrene gel was used in adsorption of Pluronic L35 surfactant at two bulk concentrations of 0.1 and 5 wt %, respectively, below and above the CMC (1 wt %). A 10 mL aqueous solution at desired surfactant concentration was prepared and a sPS gel specimen was dipped to adsorb the surfactant over a period of 24 h. The sPS gel along with adsorbed surfactant was subsequently placed in 10 mL of DI water and kept for 24 h to allow possible desorption of the surfactant from the gel at room temperature. The surface tension of this water was then measured to obtain the amount of surfactant released by the gel using σ versus surfactant concentration calibration curve.

3. RESULTS AND DISCUSSIONS

3.1. Surfactant Adsorption onto Polymer Gels. The surfactant adsorption experiments were conducted by dipping

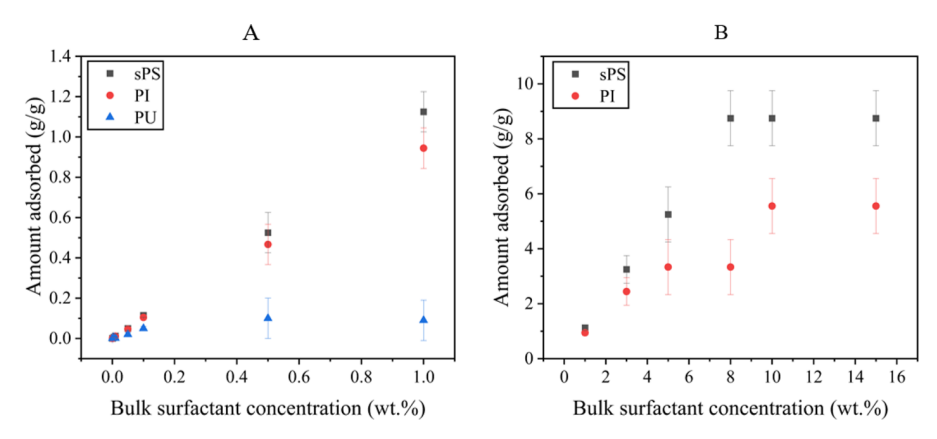


Figure 1. Pluronic L35 surfactant adsorption by sPS, PI, and PUA gels at 25 °C. (A) Bulk surfactant concentration below CMC and (B) bulk surfactant concentration above CMC.

water-filled gels of sPS, PI, and PUA of known solid mass in aqueous solutions of Pluronic L35 surfactant for a prescribed time followed by analysis of the surface tension values of the aqueous phase. The concentration of the surfactant in aqueous phase was inferred from a calibration curve of σ vs surfactant concentration, as presented in Figure S1. The calibration curve was obtained in the absence of any gel; therefore, Figure S1 applies to all gels considered in this work. The amount of surfactant adsorbed by the gel was obtained from the difference of original and residual quantities of the surfactant in the aqueous phase.

It is noted that the surfactant molecules can assume two structurally different regimes in aqueous solutions based on concentration. In regime I at low bulk concentrations (C_{bulk}), the surfactant molecules are present as unimers or isolated molecules, and in regime II they are predominantly present as aggregated structures known as micelles as the surfactant concentration goes beyond the critical micelle concentration (CMC). Above the CMC, the micellar structure is thermodynamically favored in aqueous solutions. The CMC for Pluronic L35 surfactant was found to be 1 wt %, as reflected from Figure S1. This value of CMC is corroborated by data reported elsewhere. In view of this, the surfactant solutions below and above the CMC were prepared and the surfactant—polymer gel interactions were studied.

At $C_{\rm bulk}$ below CMC, the amount of Pluronic L35 surfactant adsorbed was low, at less than 1.2 g/g, as seen in Figure 1A. Among the three gels, sPS gels adsorbed slightly higher amounts of surfactant than PI, while PUA gels adsorbed very small quantities of the surfactant, at less than 0.1 g/g. At CMC, for example, at 1 wt % surfactant, sPS, PI, and PUA gels adsorbed, respectively, 1.1, 0.95, and 0.09 g/g of surfactant. The possible factors for low surfactant adsorption amount by PUA gels will be discussed later. At or above CMC, the surfactant adsorption amount for sPS and PI were much greater than observed below CMC, for example, in the range of 1–9 g/g for sPS gel and 1–6 g/g for PI gels for surfactant concentrations in the range of 1–15 wt %. Such data are presented in Figure 1B. It is noted that PUA gels did not show additional adsorption at concentrations above the CMC.

We realized that the use of σ versus concentration calibration curves presented in Figure S1 might not have enough sensitivity to determine and analyze the extent of surfactant adsorption at above the CMC values. As an alternative, we resorted to estimation of surfactant adsorption

by the gel using solution NMR data (Figure S2). Figure 2 presents surfactant adsorption amounts on polymer gel

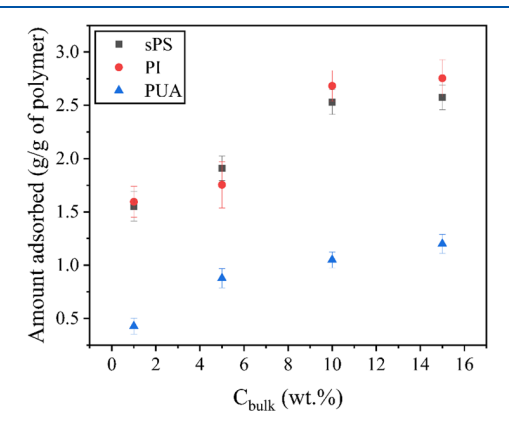


Figure 2. Surfactant adsorbed by the polymer gels calculated using 1 H NMR spectra at different values of C_{bulk} .

specimens from solution NMR data. The ¹H NMR spectra for the three gels at different Pluronic L35 surfactant concentrations can be found in Figure S3.

A large difference in surfactant adsorption amounts by the gels inferred from surface tension vs concentration data and from ¹H NMR data is clearly evident.

The surfactant adsorption amounts inferred from σ versus C_{bulk} calibration curve and that from NMR come close at or below CMC of 1 wt % surfactant concentration. However, above CMC, the difference between the two data sets widened. For example, surfactant adsorption amount by PUA gels above CMC was not sensitive to C_{bulk} with a maximum adsorbed amount of 0.09 g/g at or beyond C_{bulk} of 1 wt % (Figure 1B). However, as seen in Figure 2, the amount of surfactant adsorbed inferred from NMR data continued to increase with C_{bulk} from ~ 0.5 g/g at C_{bulk} of 1 wt % to ~ 1.2 g/g at C_{bulk} of 15 wt %. The adsorption capacity from NMR data at C_{bulk} of 15 wt % was 2.6 g/g for sPS and 2.7 g/g for PI compared to 9 g/g for sPS and 6 g/g for PI obtained as inferred from σ versus C_{bulk} calibration curve. In the rest of this work, therefore, we resorted to the use of σ versus C_{bulk} calibration curve at surfactant concentration below CMC for its convenience and for C_{bulk} above CMC, we used NMR data for its higher sensitivity.

We now examine a few questions on surfactant adsorption by water-filled gels as reflected from the data presented in Figures 1 and 2. First, what is the driving force for surfactant adsorption onto polymer gels? Second, why different polymer systems offer different adsorption capacity for the same surfactant? Third, why does the surfactant adsorption dynamics depend on surfactant concentration? One can easily conceive two driving forces that govern surfactant adsorption onto polymer gels. First is the concentration gradient of the surfactant between the bulk aqueous phase and the internal pores in the gel that drives surfactant molecule diffusion into the gel until an equilibrium is reached. The second driving force is the favorable free energy change associated with transfer of the surfactant molecules from the aqueous solutions to the polymer-water interfaces. 45 The favorable surfactantpolymer interactions are responsible for reduction of the net free energy of the system and may originate from electrostatic interactions, covalent bonding, hydrogen bonding, or hydrophobic-hydrophobic interactions between the surfactant and the polymer. 46 Therefore, to understand the driving force for surfactant adsorption, the effective concentration (C_{eff}) of the surfactant within the polymer gel was compared with the values of C_{bulk} .

The value of $C_{\rm eff}$ within the gel was calculated from the amount of surfactant adsorbed by the gel and the amount of water present within the gel. The amount of water within the gel was calculated from the total pore volume of the gel assuming that the pores were completely filled with water. The total pore volume was obtained from the product of volume of the aerogel and the porosity given in eq 1.

The total pore volumes of three types of aerogels are listed in Table 1. As an example, the effective concentration of

Table 1. Bulk Density, Skeletal Density, % Porosity, and Total Pore Volume of sPS, PI, and PUA Aerogels

polymer aerogel	bulk density (g/cm³)	skeletal density (g/cm³)	porosity (%)	total pore volume (cm^3/g)
sPS	0.08	1.05	93	11.5
PI	0.07	1.36	95	14.6
PUA	0.12	1.25	90	7.5

surfactant within the sPS gel dipped in a 0.5 wt % surfactant solution, that is, below the CMC, is calculated as follows. In this case, the total pore volume of sPS aerogel was 11.5 cm³/g, porosity of 93% (Table 1) and the amount of surfactant

adsorbed by the sPS gel was 0.53 ± 0.1 g/g (Figure 1A). In view of the above, the value of $C_{\rm eff}$ was found to be 4.6 wt %, which is 4.6 times the CMC. When the bulk surfactant concentration was above CMC, the surfactant concentration within the gel was determined from integration of the area under the peaks in the proton NMR spectrum for the surfactant and water. The analysis is elaborated in Figure S2.

The data presented in Figure 3A,B show that the value of $C_{\rm eff}$ in the gel strongly depended on the type of polymer gel used in addition to the value of $C_{\rm bulk}$. For $C_{\rm bulk} < {\rm CMC}$, for example, 0.5 wt %, the value of $C_{\rm eff}$ was 9, 6, and 2 times the $C_{\rm bulk}$ for gels of sPS, PI, and PUA, respectively, with PUA gels adsorbing the least amount among three gels. At above CMC, the ratio of $C_{\rm eff}$ and $C_{\rm bulk}$ was much smaller, for example, for a 10 wt % bulk surfactant solution, the value of $C_{\rm eff}$ in the gel was approximately 2 times the $C_{\rm bulk}$ for sPS and PI and 1.4 times the $C_{\rm bulk}$ for polyurea.

In all cases, higher values of $C_{\rm eff}$ than $C_{\rm bulk}$ indicate a reduction of free energy of the system originating from favorable interactions between the surfactant molecules and the polymer gel surface. The relatively lower values of $C_{\rm eff}/C_{\rm bulk}$ ratio at or above CMC than below CMC indicates a reduction of driving force, suggesting a distinct change of the dynamics of surfactant adsorption at $C_{\rm bulk}$ below and above the CMC.

To understand the above trend, we need to examine the trend of surfactant adsorption by the three polymer gels. Surfactants have a natural tendency to concentrate at the interfaces due to their unique structures, for example, welldefined hydrophilic and hydrophobic segments. 43 The preferential location of a surfactant at the polymer-water interface minimizes interfacial energy of the system. In this context, a polymer with higher interfacial energy with water may show higher extent of surfactant adsorption. Vijayendran et al.47 studied adsorption of an ionic surfactant, sodium dodecyl sulfate, on polymers of varying polarity values and observed that polymer-water interfacial energy had strong influence on the amount of surfactant adsorbed. To corroborate the observations of other researchers, the surfactant-polymer gel interfacial energy was calculated from the values of polymer surface energy and water contact angle values on polymer surfaces. These results are summarized in Table 2. The images of water droplets showing contact angle are found in Figure S4. The data in Table 2 show that sPS had the highest interfacial energy (48.3 mN/m) with water followed by PI (28.7 mN/m) and PUA (13.7 mN/m). This

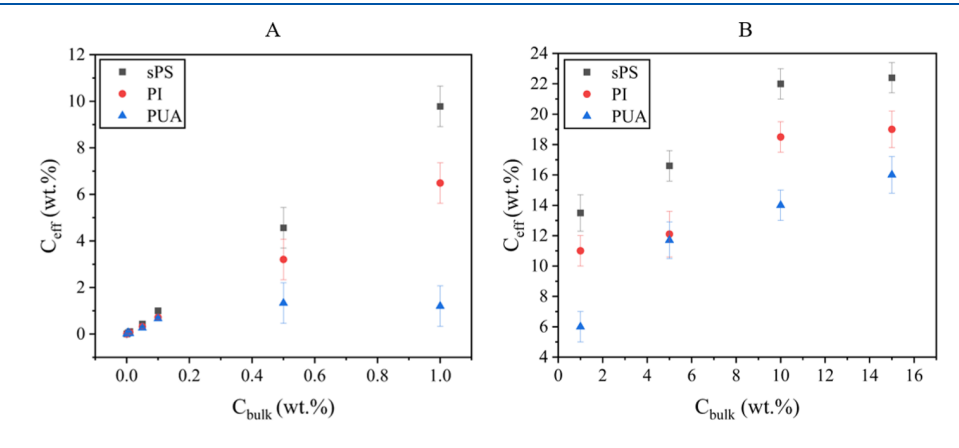


Figure 3. $C_{\rm eff}$ as a function of $C_{\rm bulk}$: (A) below and (B) above CMC for sPS, PI, and PUA.

Table 2. Surface Energy of sPS, PI, and PUA Polymer Gels Along with Their Interfacial Energy with Water

polymer	water contact angle (°)	diiodomethane contact angle $(^\circ)$	polar component (mN/m)	dispersive component (mN/m)	polymer surface energy (mN/m)	interfacial energy (mN/m)
sPS	96 ± 1	41 ± 2	2.3	38.5	40.8	48.3
PI	77 ± 2	32 ± 3	10.6	34.4	45.1	28.7
PUA	64 ± 2	48 ± 1	19.9	25.5	45.5	13.7

trend of interfacial energy values supports highest amount of surfactant adsorbed by sPS gels among the three gels used in this work

We now analyze the amounts of surfactant adsorbed by the gels in reference to what was reported in literature from earlier work. Prior work reported adsorption of surfactants on various porous and nonporous solid materials in the form of cylindrical nanoporous silica gels, colloidal silica—alumina, and polystyrene latex. $^{11,12,48-51}$ Martin et al. reported extremely low maximum amount of adsorption (0.08–0.092 g/g) for different PEO-PPO-PEO block copolymer surfactants on colloidal silica particles, 51 whereas other surfactant—polymer surface systems studied reported adsorption amounts <0.3–0.5 g/g. 9,12,48,51 These are 1 or 2 orders of magnitude lower than what are being reported in this work.

The higher extent of surfactant adsorption in the present study is attributed to higher specific surface area of the gels and the presence of confined geometry. The BET surface area and the fractions of macro- and mesopores of the three gels are listed in Table 3. The BET surface area for sPS, PI, and PUA

Table 3. BET Surface Area and Meso- and Macropore Volume Fraction of the Aerogels

polymer	BET surface area (m²/g)	total pore volume (cm^3/g)	mesopore fraction (2-50 nm)	macropore fraction (>50 nm)
sPS	260 ± 20	11.5	0.05	0.95
PI	614 ± 15	14.6	0.11	0.89
PUA	263 ± 15	7.5	0.10	0.90

aerogels were respectively 260, 614, and 263 m²/g and the corresponding BET adsorption isotherms of the three aerogels are available in Figure S5. In terms of the specific surface area alone, PI gels should account for twice as much adsorption as sPS gels. However, the much higher adsorption observed for sPS gels are attributed to much higher interfacial surface energy than PI.

PI and PUA gels used in this work had similar mesomacropore volume fractions while the mesopore fraction of sPS gel was the lowest (0.05), as listed in Table 3. The micelle size of the Pluronic L35 surfactant used with the three gels was reported to be ~2.75 nm (see Table 4). These micelles are much smaller compared to the most probable mesopore size (typically 30 nm) and all macropores contained in the gels. A set of representative SEM images in Figure 4 show appreciable open pores of size in the range of 100–300 nm for supercritically dried sPS aerogel (Figure 4A) and 10–100

nm for PI aerogel (Figure 4B). These pores would not present much size exclusion possibility for the much smaller micelles. Accordingly, the relative fractions of pores in meso- and macropore categories in the gels would not have much distinctive effects on surfactant adsorption amounts. However, the mesopore fractions of the gel may certainly influence the structural assembly of the surfactants once within the pores due to confinement effects and molecular packing. A thorough analysis of the confinement effects offered by meso- and macropores is beyond the scope of this work and will be pursued in a future study.

Another question that needs to be answered is the structural configuration of the PEO-PPO-PEO block copolymer surfactant molecules at the polymer gel-water interface at C_{bulk} below the CMC. The nature of the adsorption isotherm is generally used to identify the adsorption mechanism and to describe the structural features of the adsorbed surfactant molecules. 43 Below the CMC, the adsorption isotherm for Pluronic L35 surfactant showed a linear relationship between the amount adsorbed and the concentration of the surfactant as presented in Figure 1A, resembling a Langmuir adsorption isotherm. This suggests that a monolayer adsorption process was followed by the surfactant with no lateral interactions between the surfactant molecules at concentrations below the CMC. The surfactant is possibly interacting with a polymer gel by the weaker hydrophobic – hydrophobic interactions between the PPO segment of the surfactant and the polymer surface. Shar et al. 50 reported such interactions between the PEO-PPO-PEO block copolymer surfactants with polystyrene latexes. Other researchers reported the formation of surfactant aggregate structures like hemimicelles or bilayers at the polymer-water interfaces characterized by a steep rise in the adsorption isotherm at a surfactant concentration below the CMC of the surfactant. 12,52 The absence of such a steep rise in adsorption isotherms below the CMC shown in Figure 1A for sPS, PI, and PUA gels therefore does not suggest such aggregative behavior.

The data from NMR spectroscopy provide useful evidence about adsorbed surfactant layers and the dynamics of this layer. ⁵³ The established model for an adsorbed layer shall consist of directly bound rigid "trains" that interact with a solid surface and of tails that do not directly interact with the surface but experience reduced mobility due to covalent bonding to the trains. ⁵³ The characteristic NMR peak width increases, leading to a broadened NMR spectrum for molecules that have reduced mobility in the liquid phase due to strong adsorption on a solid surface. The extent of peak broadening is dependent

Table 4. Measured Micelle Size of the Three Surfactants at a Concentration of 5 wt % Using DLS

surfactant	most probable size (nm); frequency (%)	most probable size (nm); frequency (%)	most probable size (nm); frequency (%)	hydrodynamic diameter (nm)
Pluronic L35	$2.75 \pm 0.5; 100$			2.75
Pluronic P123	$14 \pm 3.1; 91$	$119 \pm 13.5; 9$		14.52
Pluronic F127	$16 \pm 2; 46.7$	$135 \pm 4.9; 43$	$3.6 \pm 0.35; 10$	36.82

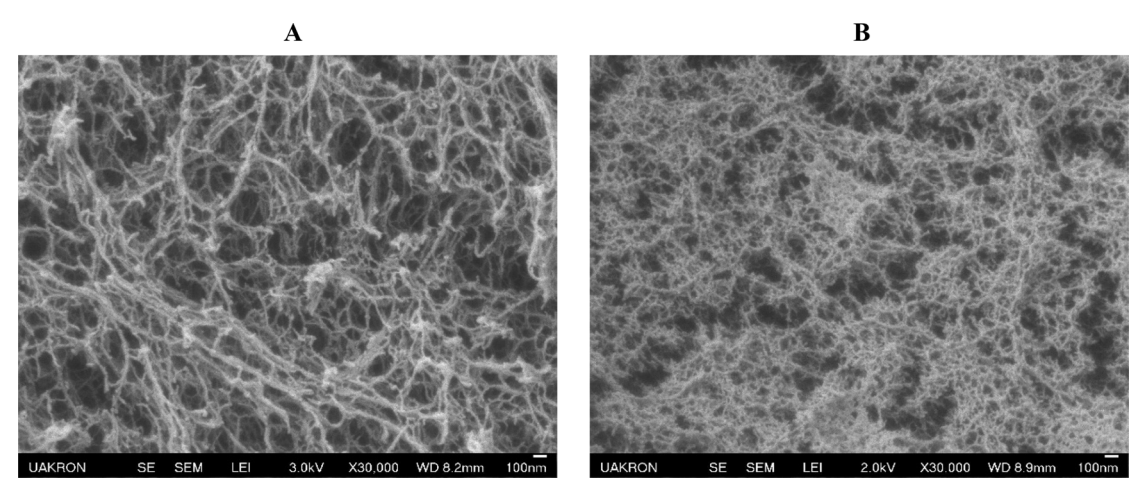


Figure 4. Representative SEM images of (A) sPS and (B) PI aerogels at 30000 magnification.

on the strength of interactions between the adsorbed layer and the adsorbent surface. Thus, we can estimate the strength of interactions between the gel surfaces and the surfactant molecules using solution NMR data. The ¹H NMR spectra for the three polymer gels at a bulk surfactant concentration of 0.1 wt % are shown in Figure 5, along with the spectrum for Pluronic L-35 surfactant solution at the same concentration.

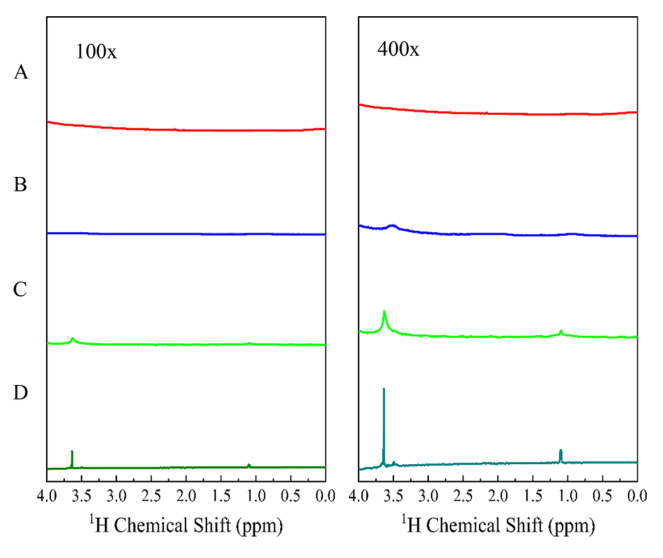


Figure 5. ¹H NMR spectra at 100× and 400× magnification for the Pluronic L35 surfactant adsorbed on (A) sPS, (B) PI, (C) PUA, and (D) Pluronic L35 surfactant at 0.1 wt % bulk concentration in DI water.

PEO-PPO-PEO block copolymer surfactants have three proton NMR peaks around 3.6, 3.50, and 1.1 ppm for the EO (-CH₂), PO (-CH₂), and PO (CH₃), respectively.⁵⁴ Sharp proton NMR peaks at these positions for the Pluronic L35 surfactant can be seen in Figure 5D. The NMR spectrum of adsorbed surfactant on the sPS gel (Figure 5A) do not show surfactant peaks at the above-mentioned positions. This suggests significant broadening of the surfactant proton signals due to strong interactions of the surfactants with polymer gels with almost a solid-like layer with reduced mobility in the aqueous phase. In case of PI gels (Figure 5B), slightly broadened peaks are visible in the spectrum indicating relatively higher degree of mobility of surfactant molecules

and, hence, relatively weaker interactions with PI gel in comparison to what was observed for sPS gels. In the case of PUA gels (Figure 5C), the peaks are relatively sharper and hence suggest an even weaker interaction of surfactant molecules with the gel surface. This tells us that the interfacial energy at the polymer gel—water interface does play a significant role in determining the intensity of interaction of the surfactant molecule with the polymer gel.

Another interesting observation was the amount of surfactant adsorbed by the gels at concentrations above the CMC. To the best of our knowledge, all the works reported on surfactant adsorption showed that the adsorption ability of the material reached a saturation value above the CMC, which means that more surfactant molecules cannot be adsorbed by the solid surface when they are predominantly present as aggregate micellar structures in a solution. ^{12,52,55} An opposite trend was observed in this study as discussed in conjunction with Figure 3. Such a trend is now further elaborated.

3.2. Surfactant Adsorption by Polymer Gels at Concentrations above the CMC. Somasundaran et al. 46 reported the thermodynamics of transfer of hydrocarbon (-CH₂) groups from a micellar environment to a solid-liquid interface. The free energy plot showed that it was not thermodynamically possible for a -CH₂ group to transfer from a highly stable micellar state to a solid-liquid interface, as the free energy of transfer would be a positive value and hence not a thermodynamically favorable process. This meant that adsorption of surfactant molecules onto the polymer surface by breaking the micellar structure would not be ideally possible. This poses a question on the possibility of a high ratio of C_{eff} and C_{bulk}, as observed in Figure 3B, and gives birth to another hypothesis to explain the surfactant adsorption above the CMC. In this hypothesis, two steps are involved. In step 1, the adsorption of the available surfactant unimers as a monolayer on the polymer surface is governed by the interfacial energy of the polymer gel-water interface, similar to an adsorption below CMC. Step 2 involves the transfer of the surfactant micelle structures within the pores of the polymer gels. The presence of the amphiphilic surfactant molecules as adsorbed molecules and micelles at the interface can possibly serve the purpose of lowering the interfacial energy of the system.

¹H NMR spectra for the sPS gels along with different Pluronic L-35 surfactant concentrations above the CMC were

obtained to estimate the level of interactions between the polymer gel and the surfactant molecules above the CMC. The NMR spectra for different values of $C_{\rm bulk}$ for sPS gels are shown in Figure 6A–E. At a $C_{\rm bulk}$ of 0.1 wt % (below CMC),

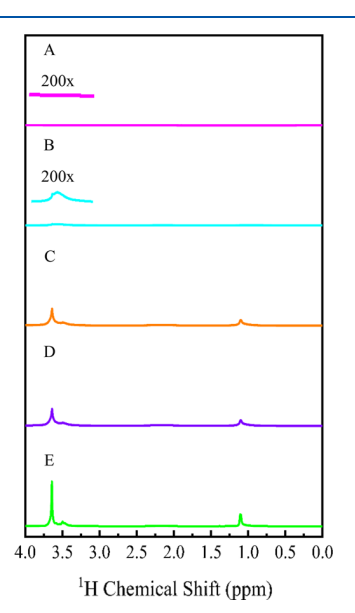


Figure 6. ¹H NMR spectra for sPS gel and Pluronic L35 surfactant at several values of C_{bulk} , curve A at 0.1 wt %, B at 1 wt %, C at 5 wt %, D at 10 wt %, and E at 15 wt %.

the absence of surfactant peaks indicate the adsorption of surfactant on polymer gel and stronger interactions between surfactant molecules. As the concentration increases to CMC and above CMC, the surfactant peaks become sharper with much reduced peak broadening indicating surfactant molecules were present dominantly in the liquid phase as a micelle. These data provide a proof for our hypothesis that surfactant micelle adsorption above the CMC occurs by the two-step process discussed above where the micelles as a whole are captured within the pores of the polymer gels.

To strengthen the hypothesis that micelle diffusion within the gel was the underlying mechanism by which surfactant adsorption occurs at concentrations above the CMC, another experiment was performed wherein three different surfactants with the same PEO-PPO-PEO block copolymer chemistry, but different micelle sizes were chosen namely Pluronic L35, Pluronic F127, and Pluronic P123.

The micelle sizes for these surfactants were measured using dynamic light scattering (DLS), and the results are reported in Table 4. The size distribution curves obtained using DLS for the three surfactants are provided in Figure S6. It is evident from Figure S6 that the micelle size distribution was bimodal for surfactants Pluronic P123 with 91% of micelles in the range of 7-25 nm and a most probable diameter of 14 nm. The remaining 9% of micelles had a broad size distribution in 80-150 nm range. The size distribution of micelles was trimodal for Pluronic F127 with approximately 10% of micelles having most probable diameter 3.6 nm, 47% of micelles having a most probable diameter of 16 nm, and the remaining 43% with the most probable diameter of 135 nm (Table 4). The mean hydrodynamic diameter calculated from the size distribution data for Pluronic L35 surfactant micelles was the lowest (2.5 nm), followed by Pluronic P123 (14.5 nm) and Pluronic F127 (36.8 nm). The measured hydrodynamic diameter for the Pluronic L35, Pluronic F127, and Pluronic P123 are in agreement with the values reported in literature. 56,57 The CMC for Pluronic P123 and Pluronic F127 were found to be around 0.1 wt % and 1 wt %, respectively.⁵⁸ sPS gels were chosen for this part of the study due to its highest surface energy being conducive for surfactant adsorption.

It is hypothesized that the size of micelles should play a dominant role in deciding surfactant adsorption if surfactant ingress into gels occurs via micelle diffusion through the porous networks, as seen in Figure 4A. In this context, surfactants with larger size micelles should experience higher resistance to diffusion through the meso- and macroporous polymer networks and hence should adsorb in lesser quantities by the gel. Figure 7A,B show the adsorbed amounts by sPS gels and the effective concentration within the sPS gels for the three surfactants. The ¹H spectrum for the sPS gel with adsorbed Pluronic F127 and Pluronic P123 are found in Figures S7 and S8.

It is seen that surfactant adsorption amounts by sPS gel follow the reverse order of the size of micelles, for example, PluronicL35 > PluronicP123 > PluronicF127 surfactant. The surfactant PluronicL35 with the smallest size micelles (2.75 nm) showed the strongest adsorption onto sPS gel, for example, 2.5 g/g and $C_{\rm eff}$ of 22 wt % at $C_{\rm bulk}$ of 10 wt %. In comparison, at the same $C_{\rm bulk}$ value, Pluronic P123 and Pluronic F127 surfactants produced respectively adsorbed

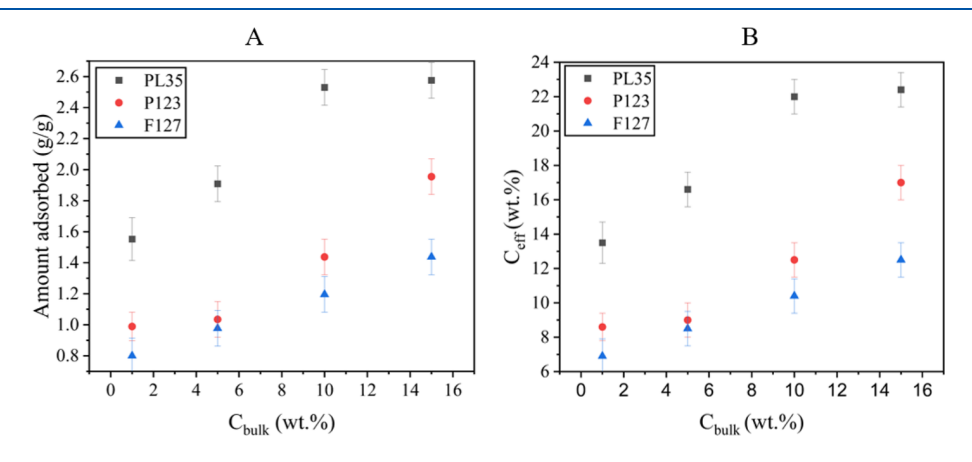


Figure 7. Pluronic L35, Pluronic P123, and Pluronic F127 surfactants: (A) adsorption by the sPS gel; (B) Ceff within the sPS gel.

quantities of 1.4 g/g and 1.2 g/g and $C_{\rm eff}$ of 12.5 and 10.4 wt %. It is noted that $C_{\rm bulk}$ was well above the respective CMC values. These data support our hypothesis that micelle diffusion and confinement of micelles into aggregate structures within the gel network are two mechanisms of surfactant adsorption by the gels when $C_{\rm bulk}$ is above the CMC values.

3.3. Desorption of Surfactant Once Adsorbed by the Polymer Gel. It is important to understand if surfactant molecule adsorption by the gel is irreversible at a C_{bulk} below CMC. In addition, it is important to understand if confinement of micelles within the gel network at a C_{bulk} above CMC is irreversible. We examined the above possibilities using sPS gel-Pluronic L35 system by placing sPS gel with previously adsorbed surfactant into DI water, as described in section 2.5.8. Table 5 lists the amounts of surfactant released by the gel upon dipping in water.

Table 5. Amounts of Pluronic L35 Surfactant Desorbed by sPS Gel

	$C_{\text{bulk}}(\text{wt }\%)$	amt of surfactant released by the gel (wt $\%$)
below CMC	0.1	~0
above CMC	5	~0.001

It is observed from the data in Table 5 that the amount of surfactant desorbed from sPS gel is negligible. Accordingly, one can infer that the surfactant irreversibly adsorbed onto the gel at concentration below CMC. At above CMC, approximately 0.001 wt % of surfactant was released into DI water which is negligibly small compared to the adsorbed amounts as previously discussed. Accordingly, it is inferred that at above CMC, the surfactant molecules were predominantly confined within the pores of the gel as micelle aggregates and such aggregation was irreversible.

4. CONCLUSION

The data presented in this paper indicate that high surface area polymer gels with meso- and macropores can strongly adsorb nanometer-sized surfactant molecules driven by high specific surface area and high surface energy values. The gels derived from sPS, PI, and PUA present an array of interfacial energies with water and accordingly show a distinct surfactant adsorption behavior. The data from ¹H NMR spectra and surface tension measurements established two distinct regimes of surfactant adsorption: as a monolayer on the gel surface below CMC and as trapped micelles within the pores of polymer gel above CMC. Both regimes were found to be irreversible. At above CMC, the amount of adsorbed surfactant reduced with an increase in the size of the micelles, indicating a strong role of micelle diffusion through the pores in the gel. Future research is needed to understand the structural dynamics of surfactants within confined geometries of the pores.

■ ASSOCIATED CONTENT

Supporting Information

The Supporting Information is available free of charge at https://pubs.acs.org/doi/10.1021/acs.langmuir.2c02198.

Additional data on the calibration curve, NMR and associated calculations, BET, and water contact angle (PDF)

AUTHOR INFORMATION

Corresponding Author

Sadhan C. Jana — School of Polymer Science and Polymer Engineering, The University of Akron, Akron, Ohio 44325, United States; orcid.org/0000-0001-8962-380X; Email: janas@uakron.edu

Authors

Pratik S. Gotad — School of Polymer Science and Polymer Engineering, The University of Akron, Akron, Ohio 44325, United States

Navin Kafle – School of Polymer Science and Polymer Engineering, The University of Akron, Akron, Ohio 44325, United States

Toshikazu Miyoshi — School of Polymer Science and Polymer Engineering, The University of Akron, Akron, Ohio 44325, United States; orcid.org/0000-0001-8344-9687

Complete contact information is available at: https://pubs.acs.org/10.1021/acs.langmuir.2c02198

Notes

The authors declare no competing financial interest.

ACKNOWLEDGMENTS

This work was partially supported by ACS Petroleum Research Fund under Grant Number PRF# 59000-ND7, U.S. National Science Foundation under Grant Number CMMI 1826030, and industrial members of Coalescence Filtration Nanofibers Consortium at The University of Akron. The raw/processed data required to reproduce these findings cannot be shared at this time as the data also forms part of an ongoing study.

■ REFERENCES

- (1) Qin, D.; Liu, Z.; Bai, H.; Sun, D. D.; Song, X. A New Nano-Engineered Hierarchical Membrane for Concurrent Removal of Surfactant and Oil from Oil-in-Water Nanoemulsion. *Sci. Rep* **2016**, *6* (1), 24365.
- (2) Wang, D.; McLaughlin, E.; Pfeffer, R.; Lin, Y. S. Adsorption of Oils from Pure Liquid and Oil–Water Emulsion on Hydrophobic Silica Aerogels. *Sep. Purif. Technol.* **2012**, *99*, 28–35.
- (3) Lee, J. H.; Kopecek, J.; Andrade, J. D. Protein-Resistant Surfaces Prepared by PEO-Containing Block Copolymer Surfactants. *J. Biomed. Mater. Res.* **1989**, 23 (3), 351–368.
- (4) Zhang, R.; Somasundaran, P. Advances in Adsorption of Surfactants and Their Mixtures at Solid/Solution Interfaces. *Adv. Colloid Interface Sci.* **2006**, 123–126, 213–229.
- (5) Micellar Liquid Chromatography; Taylor & Francis Group, CRC Press, 2000.
- (6) Schwarze, M. Micellar-Enhanced Ultrafiltration (MEUF) State of the Art. *Environ. Sci.: Water Res. Technol.* **2017**, 3 (4), 598–624.
- (7) Tiberg, F. Physical Characterization of Non-Ionic Surfactant Layers Adsorbed at Hydrophilic and Hydrophobic Solid Surfaces by Time-Resolved Ellipsometry. *Faraday Trans.* **1996**, *9*2 (4), 531.
- (8) Xu, S.-L.; Wang, C.; Zeng, Q.-D.; Wu, P.; Wang, Z.-G.; Yan, H.-K.; Bai, C.-L. Self-Assembly of Cationic Surfactants on a Graphite Surface Studied by STM. *Langmuir* **2002**, *18* (3), 657–660.
- (9) Lugo, D.; Oberdisse, J.; Karg, M.; Schweins, R.; Findenegg, G. H. Surface Aggregate Structure of Nonionic Surfactants on Silica Nanoparticles. *Soft Matter* **2009**, *5* (15), 2928–2936.
- (10) Lugo, D. M.; Oberdisse, J.; Lapp, A.; Findenegg, G. H. Effect of Nanoparticle Size on the Morphology of Adsorbed Surfactant Layers. *J. Phys. Chem. B* **2010**, *114* (12), 4183–4191.
- (11) Brumaru, C.; Geng, M. L. Interaction of Surfactants with Hydrophobic Surfaces in Nanopores. *Langmuir* **2010**, 26 (24), 19091–19099.

- (12) Shin, T. G.; Müter, D.; Meissner, J.; Paris, O.; Findenegg, G. H. Structural Characterization of Surfactant Aggregates Adsorbed in Cylindrical Silica Nanopores. *Langmuir* **2011**, *27* (9), 5252–5263.
- (13) Giordano, F.; Denoyel, R.; Rouquerol, J. Influence of Porosity on the Adsorption of a Non-Ionic Surfactant on Silica. *Colloids Surf., A* **1993**, 71 (3), 293–298.
- (14) Müter, D.; Shin, T.; Demé, B.; Fratzl, P.; Paris, O.; Findenegg, G. H. Surfactant Self-Assembly in Cylindrical Silica Nanopores. *J. Phys. Chem. Lett.* **2010**, *1* (9), 1442–1446.
- (15) Wanless, E. J.; Ducker, W. A. Organization of Sodium Dodecyl Sulfate at the Graphite–Solution Interface. *J. Phys. Chem.* **1996**, *100* (8), 3207–3214.
- (16) Zhu, B.-Y.; Gu, T. Surfactant Adsorption at Solid-Liquid Interfaces. *Adv. Colloid Interface Sci.* **1991**, 37 (1), 1–32.
- (17) Meador, M. A. B.; Malow, E. J.; Silva, R.; Wright, S.; Quade, D.; Vivod, S. L.; Guo, H.; Guo, J.; Cakmak, M. Mechanically Strong, Flexible Polyimide Aerogels Cross-Linked with Aromatic Triamine. ACS Appl. Mater. Interfaces 2012, 4 (2), 536–544.
- (18) Shinko, A.; Jana, S. C.; Meador, M. A. Crosslinked Polyurea Aerogels with Controlled Porosity. *RSC Adv.* **2015**, *5* (127), 105329–105338.
- (19) Lin, W.-H.; Jana, S. C. Analysis of Porous Structures of Cellulose Aerogel Monoliths and Microparticles. *Microporous Mesoporous Mater.* **2021**, *310*, 110625.
- (20) Kim, S. J.; Raut, P.; Jana, S. C.; Chase, G. Electrostatically Active Polymer Hybrid Aerogels for Airborne Nanoparticle Filtration. *ACS Appl. Mater. Interfaces* **2017**, *9* (7), 6401–6410.
- (21) Kulkarni, A.; Jana, S. C. Surfactant-Free Syndiotactic Polystyrene Aerogel Foams via Pickering Emulsion. *Polymer* **2021**, 212, 123125.
- (22) Teo, N.; Jana, S. C. Solvent Effects on Tuning Pore Structures in Polyimide Aerogels. *Langmuir* **2018**, 34 (29), 8581–8590.
- (23) Mawhinney, K.; Jana, S. C. Design of Emulsion-Templated Mesoporous—Macroporous Polyurea Gels and Aerogels. *ACS Appl. Polym. Mater.* **2019**, *1* (11), 3115–3129.
- (24) Daniel, C.; Giudice, S.; Guerra, G. Syndiotatic Polystyrene Aerogels with β , γ , and ε Crystalline Phases. *Chem. Mater.* **2009**, 21 (6), 1028–1034.
- (25) Guo, H.; Meador, M. A. B.; McCorkle, L.; Quade, D. J.; Guo, J.; Hamilton, B.; Cakmak, M.; Sprowl, G. Polyimide Aerogels Cross-Linked through Amine Functionalized Polyoligomeric Silsesquioxane. *ACS Appl. Mater. Interfaces* **2011**, *3* (2), 546–552.
- (26) Biesmans, G.; Randall, D.; Francais, E.; Perrut, M. Polyurethane-Based Aerogels for Use as Environmentally Acceptable Super Insulants in the Future Appliance Market. *Journal of Cellular Plastics* 1998, 34 (5), 396–411.
- (27) Teo, N.; Jana, S. C. Open Cell Aerogel Foams via Emulsion Templating. *Langmuir* **2017**, *33* (44), 12729–12738.
- (28) Wang, X.; Jana, S. C. Synergistic Hybrid Organic–Inorganic Aerogels. ACS Appl. Mater. Interfaces 2013, 5 (13), 6423–6429.
- (29) Jin, C.; Kulkarni, A.; Teo, N.; Jana, S. C. Fabrication of Pill-Shaped Polyimide Aerogel Particles Using Microfluidic Flows. *Ind. Eng. Chem. Res.* **2021**, *60* (1), 361–370.
- (30) Teo, N.; Jin, C.; Kulkarni, A.; Jana, S. C. Continuous Fabrication of Core-Shell Aerogel Microparticles Using Microfluidic Flows. *J. Colloid Interface Sci.* **2020**, *561*, 772–781.
- (31) Teo, N.; Joo, P.; Amis, E. J.; Jana, S. C. Development of Intricate Aerogel Articles Using Fused Filament Fabrication. *ACS Appl. Polym. Mater.* **2019**, *1* (7), 1749–1756.
- (32) Ghaffari Mosanenzadeh, S.; Alshrah, M.; Saadatnia, Z.; Park, C. B.; Naguib, H. E. Double Dianhydride Backbone Polyimide Aerogels with Enhanced Thermal Insulation for High-Temperature Applications. *Macromol. Mater. Eng.* **2020**, 305 (4), 1900777.
- (33) Kim, S. J.; Chase, G.; Jana, S. C. Polymer Aerogels for Efficient Removal of Airborne Nanoparticles. *Sep. Purif. Technol.* **2015**, *156*, 803–808
- (34) Daniel, C.; Alfano, D.; Venditto, V.; Cardea, S.; Reverchon, E.; Larobina, D.; Mensitieri, G.; Guerra, G. Aerogels with a Microporous Crystalline Host Phase. *Adv. Mater.* **2005**, *17* (12), 1515–1518.

- (35) Daniel, C.; Dammer, C.; Guenet, J.-M. On the Definition of Thermoreversible Gels: The Case of Syndiotactic Polystyrene. *Polymer* **1994**, 35 (19), 4243–4246.
- (36) Rhine, W.; Wang, J.; Begag, R.Polyimide Aerogels, Carbon Aerogels, and Metal Carbide Aerogels and Methods of Making Same. U.S. Patent US7074880B2, July 11, 2006.
- (37) Kawagishi, K.; Saito, H.; Furukawa, H.; Horie, K. Superior Nanoporous Polyimides via Supercritical CO₂ Drying of Jungle-Gym-Type Polyimide Gels. *Macromol. Rapid Commun.* **2007**, 28 (1), 96–100.
- (38) Rhine, W.; Wang, J.; Begag, R.Organic aerogels. U.S. Patent US5484818A, July 11, 2006.
- (39) Gu, S.; Jana, S. C. Open Cell Aerogel Foams with Hierarchical Pore Structures. *Polymer* **2017**, *125*, 1–9.
- (40) Leventis, M.; Sotiriou-Leventis, C.; Chandrasekaran, N.; Mulik, S.; Larimore, Z.; Lu, H.; Churu, G.; Mang, J. Multifunctional Polyurea Aerogels from Isocyanates and Water. A Structure—Property Case Study Chemistry of Materials. *Chem. Mater.* **2010**, 22 (24), 6692–6710.
- (41) Singh, V.; Khullar, P.; Dave, P. N.; Kaur, N. Micelles, Mixed Micelles, and Applications of Polyoxypropylene (PPO)-Polyoxyethylene (PEO)-Polyoxypropylene (PPO) Triblock Polymers. *Int. J. Ind. Chem.* **2013**, *4*, 12.
- (42) Wu, S. Calculation of Interfacial Tension in Polymer Systems. *Journal of Polymer Science Part C: Polymer Symposia* **1971**, 34 (1), 19–30
- (43) Myers, D. Surfactant Science and Technology; John Wiley & Sons, 2020.
- (44) KRUPKA, T. M.; EXNER, A. A. Structural Parameters Governing Activity of Pluronic Triblock Copolymers in Hyperthermia Cancer Therapy. *Int. J. Hyperthermia* **2011**, 27 (7), 663–671.
- (45) Davies, J. T.Interfacial Phenomena; Elsevier, 2012.
- (46) Somasundaran, P.; Shrotri, S.; Huang, L. Thermodynamics of Adsorption of Surfactants at Solid-Liquid Interface. *Pure Appl. Chem.* **1998**, 70 (3), 621–626.
- (47) Vijayendran, B. R. Polymer Polarity and Surfactant Adsorption. *J. Appl. Polym. Sci.* **1979**, 23 (3), 733–742.
- (48) Samiey, B.; Golestan, S. Adsorption of Triton X-100 on Silica Gel: Effects of Temperature and Alcohols. *Cent. Eur. J. Chem.* **2010**, 8 (2), 361–369.
- (49) Somasundaran, P.; Fuerstenau, D. W. Mechanisms of Alkyl Sulfonate Adsorption at the Alumina-Water Interface ¹. *J. Phys. Chem.* **1966**, 70 (1), 90–96.
- (50) Shar, J. A.; Obey, T. M.; Cosgrove, T. Adsorption Studies of Polyethers Part 1. Adsorption onto Hydrophobic Surfaces. *Colloids Surf., A* 1998, 136 (1), 21–33.
- (51) Malmsten, M.; Linse, P.; Cosgrove, T. Adsorption of PEO-PPO-PEO Block Copolymers at Silica. *Macromolecules* **1992**, 25 (9), 2474–2481.
- (52) Levitz, P. Aggregative Adsorption of Nonionic Surfactants onto Hydrophilic Solid/Water Interface. Relation with Bulk Micellization. *Langmuir* 1991, 7 (8), 1595–1608.
- (53) Schönhoff, M.; Larsson, A.; Welzel, P. B.; Kuckling, D. Thermoreversible Polymers Adsorbed to Colloidal Silica: A 1H NMR and DSC Study of the Phase Transition in Confined Geometry. *J. Phys. Chem. B* **2002**, *106* (32), 7800–7808.
- (54) Ma, J.; Guo, C.; Tang, Y.; Liu, H. 1H NMR Spectroscopic Investigations on the Micellization and Gelation of PEO-PPO-PEO Block Copolymers in Aqueous Solutions. *Langmuir* **2007**, 23 (19), 9596–9605.
- (55) Alexandridis, P.; Alan Hatton, T. Poly(Ethylene Oxide)-poly(Propylene Oxide)-poly(Ethylene Oxide) Block Copolymer Surfactants in Aqueous Solutions and at Interfaces: Thermodynamics, Structure, Dynamics, and Modeling. *Colloids Surf., A* **1995**, *96* (1), 1–46.
- (56) Bharatiya, B.; Ghosh, G.; Bahadur, P.; Mata, J. The Effects of Salts and Ionic Surfactants on the Micellar Structure of Tri-Block Copolymer PEO-PPO-PEO in Aqueous Solution. *J. Dispersion Sci. Technol.* **2008**, 29 (5), 696–701.

- (57) Perez-Sanchez, G.; Vicente, F. A.; Schaeffer, N.; Cardoso, I. S.; Ventura, S. P. M.; Jorge, M.; Coutinho, J. A. P. Rationalizing the Phase Behavior of Triblock- Copolymers through Experiments and Molecular Simulations. *J. Phys. Chem. C* **2019**, *123* (34), 21224–21236.
- (58) Su, Y.; Liu, H. Temperature-Dependent Solubilization of PEO-PPO-PEO Block Copolymers and Their Application for Extraction Trace Organics from Aqueous Solutions. *Korean J. Chem. Eng.* **2003**, 20 (2), 343–346.

□ Recommended by ACS

Surprising Hydrophobic Polymer Surface with a High Content of Hydrophilic Polar Groups

Mingru Li, Shengtao Li, et al.

DECEMBER 01, 2022

LANGMUIR

READ 🗹

Surface Enrichment of Polymer-Grafted Nanoparticles in a Miscible Polymer Nanocomposite

Shawn M. Maguire, Russell J. Composto, et al.

AUGUST 23, 2022

MACROMOLECULES

READ 🗹

Polymer Fractionation at an Interface in Simple Shear with Slip

Shadrach Kwakye-Nimo, Paula M. Wood-Adams, et al.

JULY 25, 2022

MACROMOLECULES

READ 🗹

Neutron Reflectivity Study on the Suppression of Interfacial Water Accumulation between a Polypropylene Thin Film and Si Substrate Using a Silane-Coupling Agent

Keisuke Shimokita, Tsukasa Miyazaki, et al.

OCTOBER 04, 2022

LANGMUIR

READ 🗹

Get More Suggestions >